The International Journal of Advanced Manufacturing Technology (2018) 97:3903–3914
https://doi.org/10.1007/s00170-018-2014-x

ORIGINAL ARTICLE

Research on removal characteristics of recast layer of laser-electrolytic machining on small holes

Xuezhi Li[1] · Jianping Zhou[1] · Kedian Wang[1,2]

Received: 26 December 2017 / Accepted: 4 April 2018 / Published online: 3 June 2018
© Springer-Verlag London Ltd., part of Springer Nature 2018

Abstract
To address defects in the recast layer and microcracks in laser drilling, this study adopted laser-electrolytic composite machining technology to conduct a boring test on nickel-based superalloy In718 through flushing outside the ring electrode and hydrostatic machining. This method obtained the characteristics of recast layer removal via composite machining and identified the influence rule of the residual rate of the recast layer via composite machining parameters. Results show that the recast layer exhibits a random distribution and gathers together at the exit when adopting the laser to rotationally cut and make the hole. Electrolytic post-processing for laser prefabricated small holes with a diameter larger than 1 mm by flushing outside the ring electrode proceeded as follows: using an electrolytic voltage of 20 V, $NaNO_3$ electrolyte of 7.5 g/L, and electrolytic machining time of 20s, the reaming amount can reach 70–100 μm and steadily achieve recast layer removal. Electrolytic post-processing for prefabricated small holes with a diameter smaller than 1 mm can be carried out using hydrostatic machining under different flushing methods (continuous static electrolyte machining, free flushing, and forced flushing), indicating that forced flushing can remove the recast layers of the holes and achieve a better hole shape to create holes with good inwall quality.

Keywords Air film cooling hole · Recast layer · Laser-electrolytic machining · Flushing outside the ring electrode · Hydrostatic machining · Technological parameter

1 Introduction

A mass of air film cooling holes with a diameter of 0.25–1.8 mm exists on key hot-end components (e.g., high-pressure turbine operating blades, guide blades, combustors, etc.) of the aero-engine. Hole machining quality is of great concern, yet with most hot-end components being manufactured with nickel-based superalloy, traditional machining methods struggle to meet the requirements [1, 2]. To realize a high thrust-weight ratio, high combustion efficiency, low emissions, and other performance standards, the hot-end components of aero-engines widely adopt air film cooling technology [3]. Air film cooling technology can enhance aero-engine performance while also presenting higher requirements for air film hole machining technology. Laser machining is the main method for preparing an air film cooling hole; however, recast layers exist around the hole wall and the area around the hole mouth, which are susceptible to microcracks, heat-affected zones, and other defects under thermal stress. These defects will reduce the service life of the parts and can even seriously influence their performance and reliability [4, 5].

To obtain high-quality small holes with few or no recast layers, domestic and foreign scholars have conducted extensive research on recast layer removal methods. Along with adopting an ultrashort pulse laser to improve laser unit performance, methods also include laser machining for subsequent finishing processing, optimal laser machining with technological parameters, auxiliary gas injection laser machining, underwater laser machining, and composite laser machining [6–17]. Nguyen MD [16] conducted a composite machining experiment involving electrochemical machining (ECM) and electrical discharge machining (EDM). Low-resistivity deionized water was selected as the electrolyte in composite machining; the aim was to exploit the advantages of EDM and ECM in terms of processing efficiency and surface quality. The results

✉ Kedian Wang
kdwang@mail.xjtu.edu.cn

[1] Department of Mechanical Engineering, Xinjiang University, Urumqi 830047, China

[2] Department of Mechanical Engineering, Xi'an Jiaotong University, Xi'an 710049, China

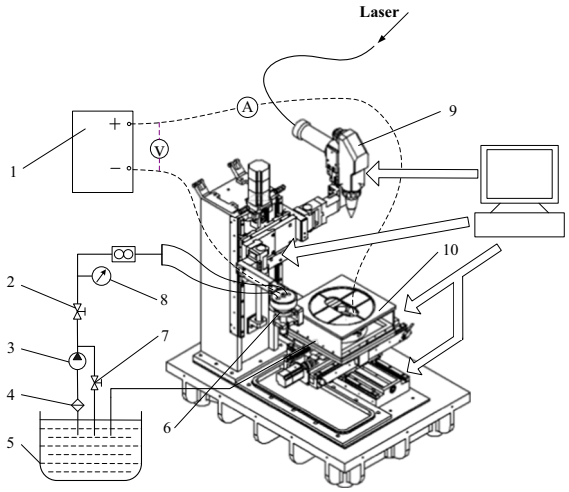

1. Power
2. Regulator
3. Stainless steel corrosion pump
4. Pre-filter
5. Electrolyte tank
6. Electrolyzing fluid device
7. Relief valve
8. Pressure gauge
9. Laser transmitter
10. Working box

Fig. 1 Experimental system structure

showed that a small hole with a diameter of φ100 μm was prepared at a frequency of 500 KHz, a duty cycle of 30%, a feed rate of 0.2 μm, and a machining time of 15 min. Qu Ningsong [18] conducted an ECM-EDM composite machining experiment to machine a nickel-based superalloy material (DZ22) through a brass electrode with a diameter of 0.5 mm. A small hole with an average aperture of 568.6 μm and average recast layer thickness of 20 μm was prepared at a pulse width of 10 μm and a peak current of 6 A. The influence of the cathode rotation and power supply mode on machining speed and machining stability was also analyzed. Finally, a small hole without a recast layer was prepared by electrolytic reaming with 200 mA constant current output. IBM in the USA [19] proposed a new machining method of laser auxiliary electrolytic machining, adopting a sodium chloride and sodium nitrate solution as the electrolyte to conduct a comparative test of micro-jet electrolysis and laser auxiliary micro-jet electrolysis on nickel-based materials using a continuous argon ion laser with a green light wave band and average power of 22 W. The results showed that the laser strengthened the electrolytic action of the machining region, reducing stray currents and stray corrosion and effectively decreasing the overcut quantity while increasing machinable hole depth. V. Lescuras [20] took sodium chloride as the electrolyte and mixed it with nitrogen, then used a laser with an average power of 1 W, frequency of 30 Hz, and wavelength of 532 nm to facilitate jet electrolytic etching and carried out a boring test on nickel material using different-sized nozzles. The results showed that the liquid jet zone was compressed under pulse laser action and enhanced the dimensional precision of the holes. The hole-type edges became smoother and sharper, the profile was clear, and the shape was regular; however, a pulse laser did not provide clear acceleration for machining efficiency. Researchers at Hong Kong Polytechnic University [21] conducted a study on ultrasonic-aided laser beam machining, which applied supersonic vibration to workpieces (aluminum-based compound materials) when carrying out laser machining with a Nd:YAG pulse laser unit at a supersonic vibration frequency of 20 kHz. The results indicated that supersonic vibration can effectively remove metal melt and enhance the depth-to-diameter ratio of the machining hole. However, high-frequency vibration can easily damage hard-brittle material parts. Xu Jiawen [22] proposed a jet ECM laser beam machining method, using a focused laser beam, to remove recast layers via the cooling, flushing, and electrolytic action of jet machining. The results showed that adopting sodium nitrate as the electrolyte, at a pressure of 1.5 MPa and concentration of 18%, can reduce recast layers by over 90%.

This study examined small-hole machining without recast layers on a nickel-based superalloy to reform and extend

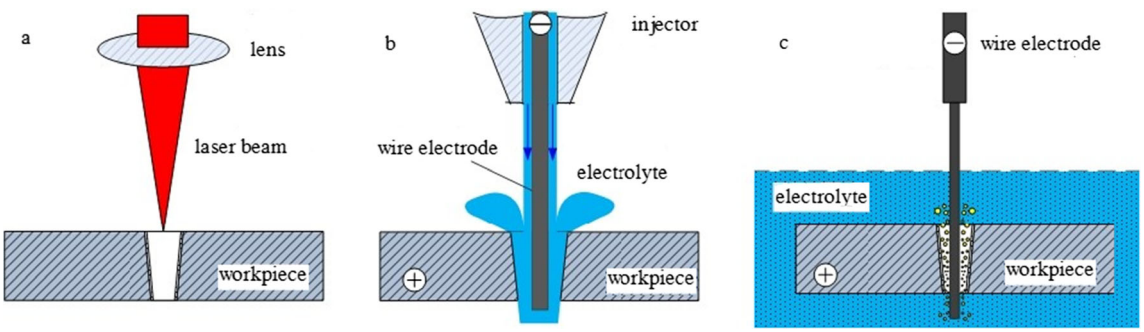

Fig. 2 Composite machining. **a** Laser roughing. **b** Flushing outside the ring electrode. **c** Hydrostatic machining

Table 1 Technological parameter

Technological parameter	Setting value
Pulse width	0.2 ms
Peak power	16 kW
Repetition rate	70 Hz
Defocusing distance	+0.2 mm
Circle diameter	Ø0.22 mm
Rotary-cut speed	0.1 mm/s
Rotary-cut number	3
Assistant gas	N_2 (0.5 MPa)
Tool electrode	Copper tube electrode with an outer diameter of 1 mm
Workpiece	In718(1 mm)

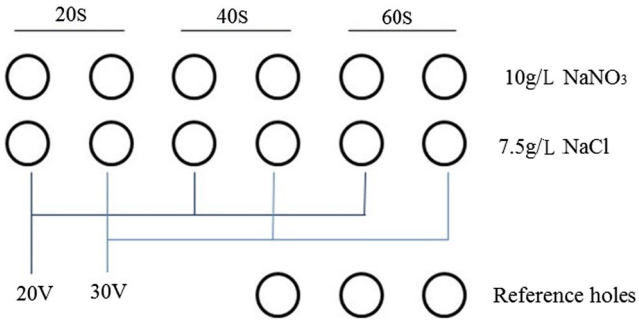

Fig. 3 Scheme of flushing outside the ring electrode

existing five-axis NC machining given a deep understanding of related mechanisms of laser machining and electrolytic machining. By adding to the electrolytic machining system components to fully leverage high-laser machining efficiency and electrolytic machining without recast layers, residual stress, and microcracks, a test was carried out for small-hole laser-electrolytic composite machining. Research on laser drilling recast layer technology by electrolytic removal has important implications for hot-end component air film cooling hole machining in aero-engines.

2 Laser-electrolytic composite machining principle

2.1 Laser-electrolytic composite machining experimental apparatus

Laser machining and electrolytic machining are forms of special machining that adopt luminous energy, heat energy, electrochemical energy, etc. to remove materials in the machining process. Compared with regular metal-cutting machine tools, the experimental system in this study has some different characteristics: no cutting force and vibration noise exist in the machining process, and the working process is stable; because of photoelectric liquid and other multimedia coupling in machining, the equipment is required to provide good corrosion resistance, insulation, and sealing. Laser machining modules include the high-power laser unit, water-chilling unit, laser launch head, and optical fiber. Electrolytic machining modules include the flushing equipment used for electrolysis (electrolytic machining head), electrolyte circulating system, and corresponding tooling equipment, which mainly operates through self-designed trial production. Figure 1 depicts the laser-electrolytic composite machining experimental system.

2.2 Laser-electrolytic composite machining scheme

This study carried out electrolytic post-processing for the recast layers formed by laser drilling and proposed a new composite machining technology, as shown in Fig. 2. The process is as follows: first, the prefabricated holes were quickly processed via laser, and then the residual machining allowance and machining defects were removed by electrolytic machining to obtain high-quality small holes without a recast layer, microcracks, and residual stress. Different electrolytic methods were adopted to remove the laser drilling recast layer according to the respective diameters of the prefabricated holes. For small holes with a diameter larger than 1 mm, flushing was used outside the ring electrode to remove the recast layers; for small holes with a diameter smaller than 1 mm, an electrode wire was easily vibrated under the liquid flow. The electrolyte could not flow fully through the gap and blocked

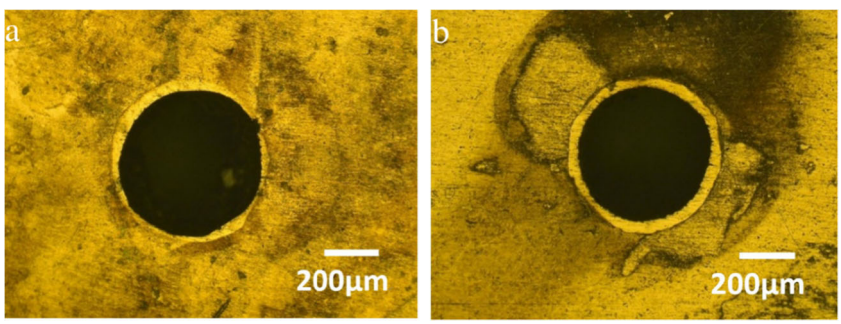

Fig. 4 Metallograph of In718. **a** Inlet. **b** Outlet

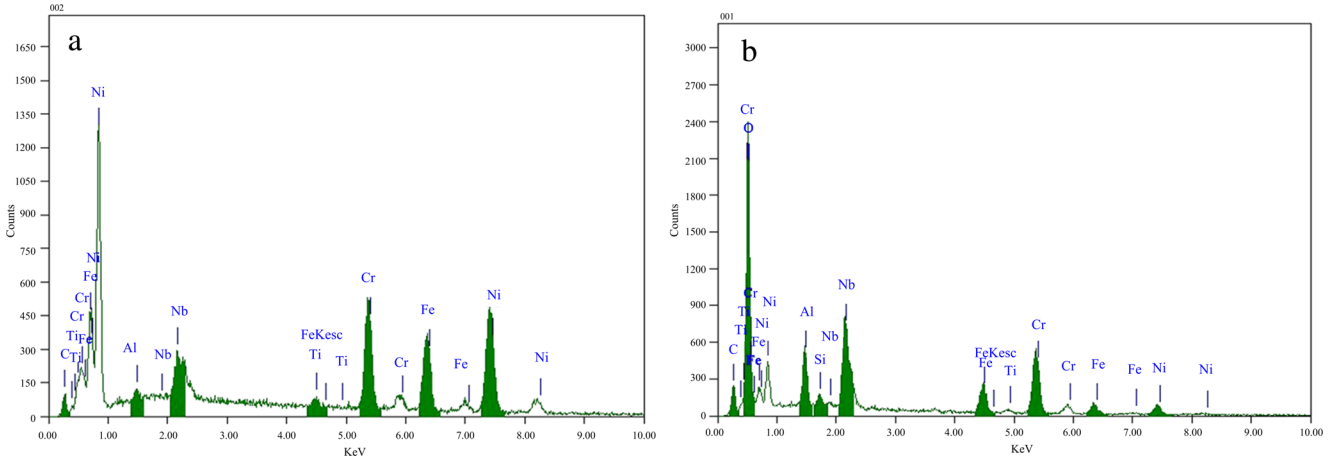

Fig. 5 EDS analysis of In718. **a** Matrix. **b** Recast layer

the electrochemical reaction from proceeding. Next, it was necessary to carry out a periodic flushing operation after cutting off the power supply using the cycle flushing hydrostatic processing method to update the electrochemical reaction environment. Then, it was possible to remove electrolytic products, generated joule heat, and electrode polarization to allow electrolysis to proceed continuously and smoothly.

2.3 Laser-electrolytic composite machining experimental conditions

A K300D laser unit was used in this study; the experimental technological parameters are shown in Table 1. Fifteen array holes with the same parameters were processed, including 12 holes that were used to examine the impact of the technological parameters of electrolytic machining; the remaining three were reference holes to be compared with any change in holes before and after electrolytic processing. In this paper, neutral electrolyte (NaCl, $NaNO_3$, and $NaClO_3$) was mainly used for electrolysis treatment to research machining characteristics of neutral salt solution. In hydrostatic machining, to obtain better nonlinearity characteristics of the electrolyte, excellent hole shape, good inner-wall quality, and hole wall without the recast layer, a compound electrolyte of neutral salt solution and acid solution can be used to remove the micro-recast layer of the hole wall.

For electrolytic machining flushing outside the ring electrode, a 7.5 g/L NaCl solution and 10 g/L $NaNO_3$ solution were mixed separately, and the feeding pressure of electrolyte was 0.1 MPa. As shown in Fig. 3, for every kind of electrolyte, the electrolytic voltage was 20 V and 30 V, respectively, to successively control the electrolyte machining time of each voltage level at 20, 40, and 60 s. To further improve the electrolyte formula under forced flushing, $NaNO_3$ served as the main body to which a small amount of $NaClO_3$ was added at a 9:1 proportion; HCl was 0.12 mol/L.

The electrolyte pressure includes the outlet pressure of the electrolyte pump and the pressure at the inlet of the machining gap. The former generally needs to be higher (0.05–0.1 MPa) than the latter given pressure loss in the flow passage. The liquid velocity range in electrochemical machining is usually 6~30 m/s, considering the actual use conditions, the center is occupied by the electrode, the electrolyte flow from the edge, its speed will also change, and the best electrolytic effect can be achieved at an exit velocity of 13.5 m/s and an average entrance pressure of 0.15 MPa. Therefore, the feeding pressure of the electrolyte is adjusted to 0.1 MPa.

3 Analysis of laser rotary-cut boring recast layer

The diameter of the inlet hole of the laser rotary-cut machining prefabricated hole was 546.48 μm. The outlet hole diameter was 404.56 μm; Fig. 4 shows the metallograph of the small-hole machining on In718. The recast layers appeared to be unequally distributed around the hole. Regarding the

Table 2 Composition comparison of In718 matrix and recast layer

Element	C	O	Al	Si	Ti	Cr	Fe	Ni	Nb
Matrix (%)	4.90	–	0.68	0.51	1.05	20.17	23.39	42.91	6.90
Recast layer (%)	7.68	43.91	3.77	0.57	4.49	13.91	3.22	4.91	17.54

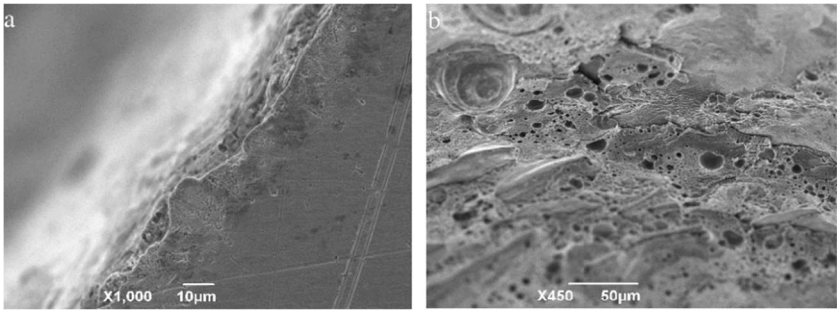

Fig. 6 Micromorphology of recast layer. **a** Shape. **b** Microcrack

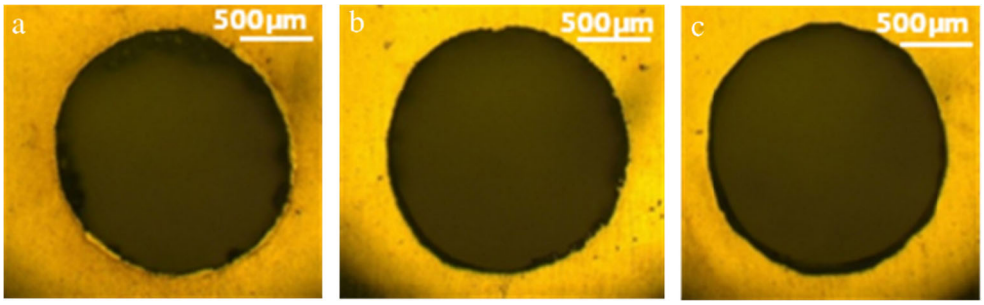

Fig. 7 Metallography before and after electrolysis. **a** Laser prefabricated hole. **b** NaCl. **c** $NaNO_3$

thickness direction, the recast layers at the inlet demonstrated a maximum value of 33.70 μm and minimum value of 12.97 μm. The recast layers at the outlet were more abundant and thicker. Results also show melt flows in the hole under a high-speed airstream with a random final stopped position. The flow was more heavily distributed at the lower part of the hole, affording the recast layer distribution a certain randomness. The layers also gathered together at the outlet.

The EDS analysis of the In718 matrix and laser drilling recast layer is presented in Fig. 5. Table 2 shows the oxidation phenomenon in the recast layers during the phase change process; the element contents of Al, Ti, Fe, Ni, O, and Nb varied greatly. This means that during the phase change, jet, and condensation process, the microstructure of the recast layers formed by melting materials changed with atom migration and recombination. The original and stable crystal lattice of the nickel-based superalloy was destroyed by these changes, and part of the strengthening phase either disappeared or transformed, which countered the exertion of the excellent working performance of the nickel-based superalloy under high temperatures. In addition, the percentage of O content in the recast layer reached 43.92%, presumably because the molten metal under the photothermal effect reacted with oxygen in the air to form oxides, resulting in a significant increase in O content. Therefore, the O element content also increased, although the N_2 auxiliary gas was adopted. Figure 6 shows the micromorphology of the recast layers on the hole wall and corresponding hairline fissures. Because the temperature gradient at the hole edge was large, the microcrystal grew along with the temperature gradient when the recast layers re-solidified. In the fine dendrite morphology, the structure's texture direction and diameter direction were perpendicular to the matrix.

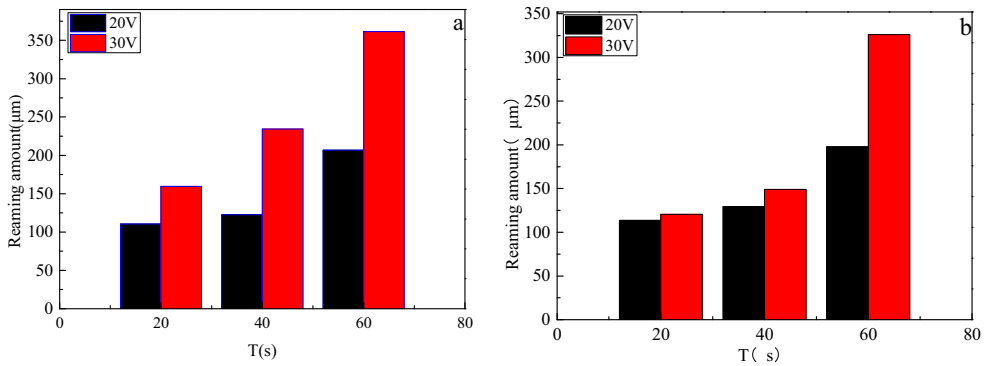

Fig. 8 Comparison of reaming amount. **a** NaCl. **b** $NaNO_3$

Table 3 Reaming amount

	Bilateral reaming amount(μm)					
	NaCl			$NaNO_3$		
	20 s	40 s	60 s	20 s	40 s	60 s
20 V	110.63	122.57	206.78	113.61	129.41	197.77
30 V	159.53	234.29	361.29	120.50	149	326

4 Recast layer removal by flushing outside the ring electrode electrolysis

First, the samples were washed with acetone after electrolysis before being ground and polished. Then, metallographic corrosion was conducted using a copper sulfate-hydrochloric acid solution. Morphologies were observed under the metallurgical microscope, and the aperture values were measured and recorded. Figure 7 shows part of the metallographic micrograph, indicating the recast layers on the laser prefabricated hole distributed around the hole. Their average thickness was 28.72 μm. The back side of the samples adhered to the burr formed by the residual melt at the outlet during the blowing process. After electrolysis, the recast layers and burr were removed, the hole roundness improved, and the surface quality appeared sound and complete.

Changes in the reaming amount after electrolysis are shown in Fig. 8 and Table 3, illustrating that the reaming amount was directly proportional to the electrolytic voltage and machining time, which increased in line with increasing electrolytic voltage and machining time. Because NaCl solution is the linear electrolyte, voltage had an obvious impact on the NaCl solution, while the current efficiency showed nearly no change. However, the voltage exerted a small effect on the $NaNO_3$ solution because the anode surface generated a passive film in the reaction process, reduced the reaction speed, and conveniently controlled the aperture dimensions. In addition, the reaming speed became faster with extended time because of the larger machining gap, the electrolyte flowed more smoothly, and the electrochemical reaction environment updated regularly.

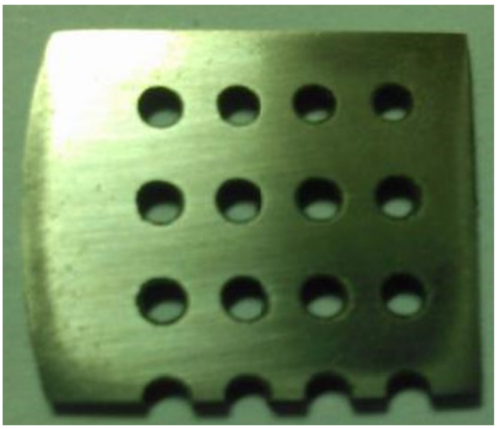

Fig. 10 Specimen

The morphology of the hole side wall after the reference hole, NaCl processing, and $NaNO_3$ processing is shown in Fig. 9. The adhesive materials on the inner wall of the hole formed by laser machining exhibited an obvious liquid-drop form, which was actually the recast layer formed by the residual melt solidifying quickly on the hole wall and distributed mainly at the lower end of the hole. The recast layer was removed after electrolytic processing, and the new surface exposed from the matrix was bright, clean, and smooth. The taper of each hole was calculated according to the measured inlet and outlet dimensions. The hole tapers in Fig. 9a–c were 0.32, 0.21, and 0.128, respectively. Compared with the NaCl electrolyte, adopting $NaNO_3$ in electrolysis further decreased the hole taper because of the non-linear characteristics of the solution. Stray corrosion had a small impact on the hole shape when carrying out electrolysis, and it appeared to enhance hole shape accuracy. The calculation formula for the hole taper is as follows:

$$C = \tan\frac{\alpha}{2} = \frac{d_{\text{enter}} - d_{\text{exit}}}{2h} \tag{1}$$

where α denotes the coning angle of the taper hole and h is the hole depth.

Based on the above analysis, when selecting $NaNO_3$ solution as the electrolyte, its concentration was 7.5 g/L. To stabilize the machining process, the laser rotary-cut

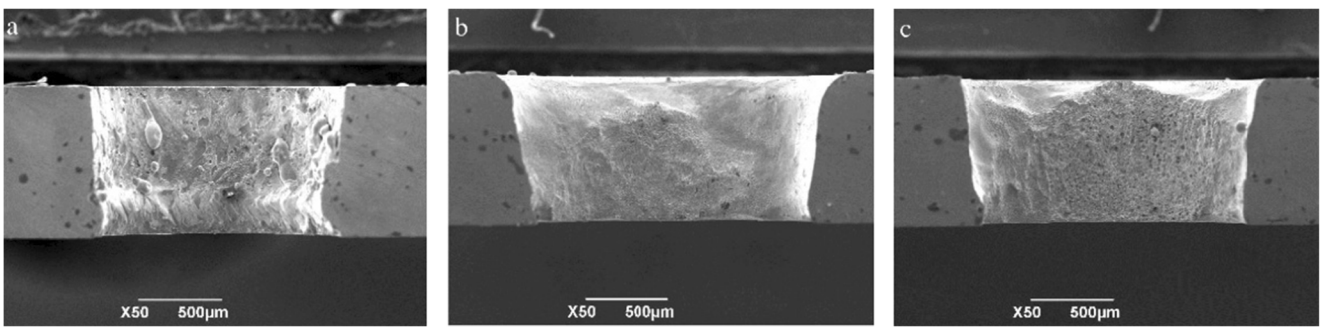

Fig. 9 Morphology of the hole side wall before and after electrolysis. **a** Laser prefabricated hole. **b** NaCl. **c** $NaNO_3$

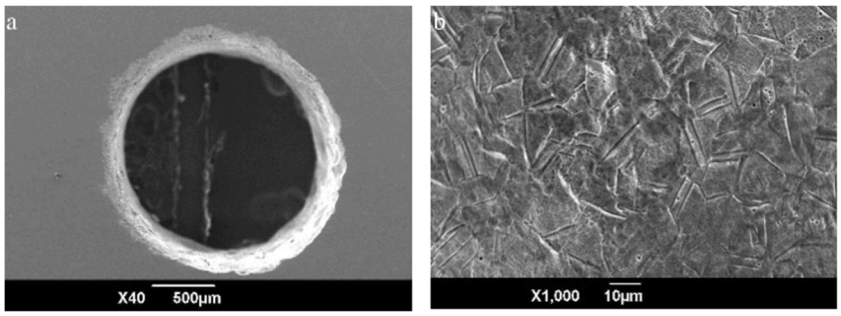

Fig. 11 Morphology of the entrance and of the inner wall. **a** Entrance. **b** Inner wall

diameter was set as Φ1.2 mm, electrolytic voltage as 20 V, and machining time as 30s. Twelve holes were processed using the same machining parameters. As shown in Fig. 10, four holes in the row were laser prefabricated before electrolytic processing, the last three rows were the experimental holes, and a longitudinal cut was made for the holes in the last row to observe the morphology of the hole wall.

The average aperture value of the prefabricated hole by laser machining was 1548 μm. The machining process was stable without a short-circuit phenomenon, and many bubbles appeared at the outlet and inlet but were eliminated from the machining gap with the liquid flow. The aperture value of all holes after electrolytic machining was similar, in the range of 1620–1650 μm. The maximum bilateral recast layer thickness did not exceed 70 μm, and the reaming amount was between 70 and 100 μm and could completely remove the recast layers. Figure 11 shows the morphology of the entrance and the inner wall of the partial hole. The small hole shape was further optimized after electrolysis, which became smoother and brighter. The matrix structure of the inner wall was distributed in a regular strip shape by the amplified observation, and the acicular dashed lines indicate the grain boundary and subgrain boundary of the inner composed phase. The material energy on the interface was higher than on the inside. The interface was the first to be corroded during electrochemical dissolution, showing a groove and narrow gap. Then, it was necessary to select the appropriate dilute aqua regia to corrode the new sample In718 and apply high-frequency vibration via an ultrasonic cleaning instrument; its metallographic structure is shown in Fig. 12. Several needle-like δ phases were found to exist in the In718 matrix and were distributed in the subgrain boundaries or in the high dislocation density region. Such crystal defects generated interfacial tension in the δ phase, resulting in the appearance of grooves in the defect position. The morphology of the inner wall was highly similar to the obtained matrix structure; therefore, the recast layer in laser drilling appears to have been completely removed after electrolytic machining.

5 Micro-recast layer removal by hydrostatic electrolytic machining

For small holes with a diameter smaller than 1 mm, as the aperture decreased, the electrode stiffness became smaller so the bending deformation became easier. In addition, the outlet size of ideal nozzle was small, but it was difficult to process. Large size nozzle outlet led to disorder of electrolyte fluency, stray corrosion, and other unfavorable factors. By continuing to use flushing outside ring electrode electrolysis, it would remain difficult to obtain better-quality holes. According to the enlightenment of the micro-ECM [10, 23, 24], this paper adopted hydrostatic machining to remove the recast layer of the hole wall.

First, an experiment with a continuous static electrolyte was carried out to investigate the effects of electrolytic voltage and machining time on hole shape and surface quality. The electrolyte was configured as a mixed solution of 20 g/L $NaNO_3$ and 0.12 mol/L HCl (diluted 100 times). The machining time was fixed to 3 min, and the electrolytic voltage was set to 5, 6, 7, 8, and 9 V; experimental

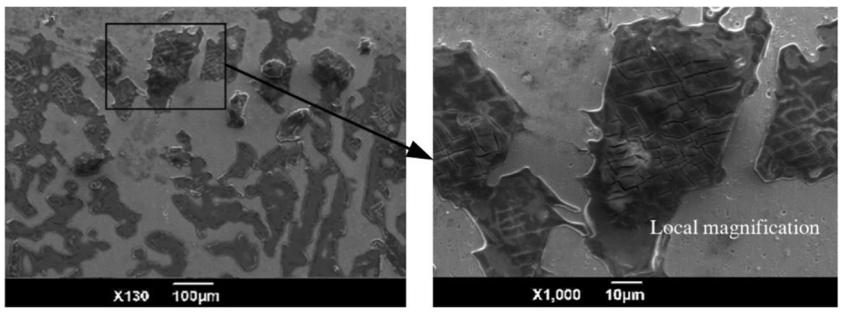

Fig. 12 In718 matrix structure

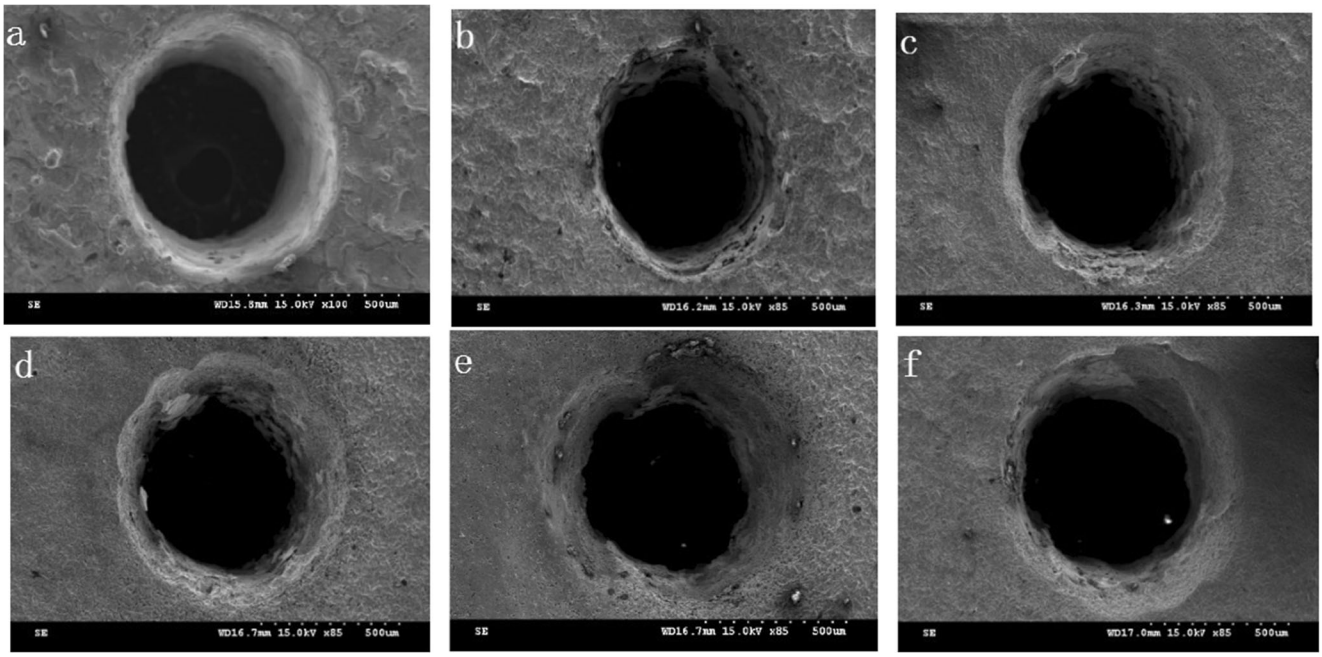

Fig. 13 The hole morphology at different voltages ($NaNO_3$ + HCl). **a** Reference hole. **b** 5 V. **c** 6 V. **d** 7 V. **e** 8 V. **f** 9 V

results appear in Fig. 13. The electrolytic voltage was set to 6 V, and the machining time was set to 2, 3, 4, and 5 min; experimental results are shown in Fig. 14.

Figures 13 and 14 indicate that the change in hole shape was smaller, hole circularity was maintained, and hole eccentricity was not clearly enlarged in hydrostatic electrolytic

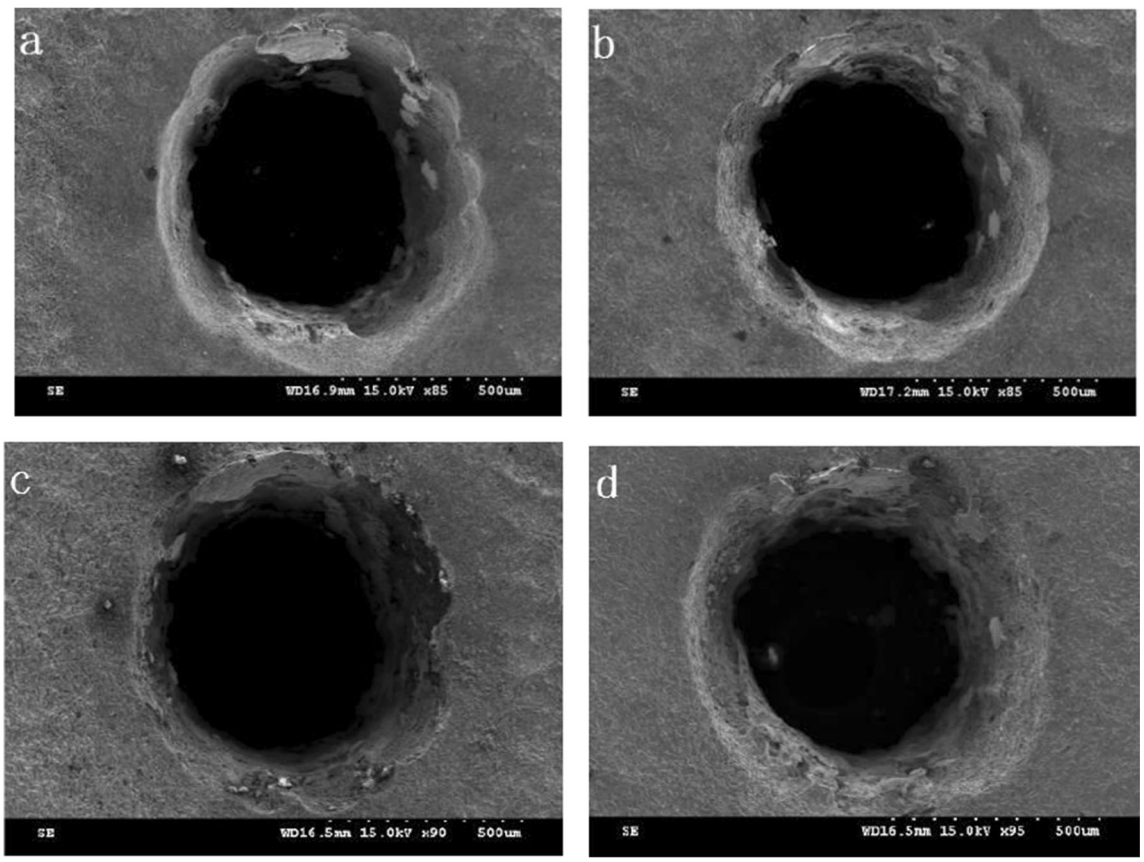

Fig. 14 The hole morphology at different times. **a** 2 min. **b** 3 min. **c**4 min. **d** 5 min

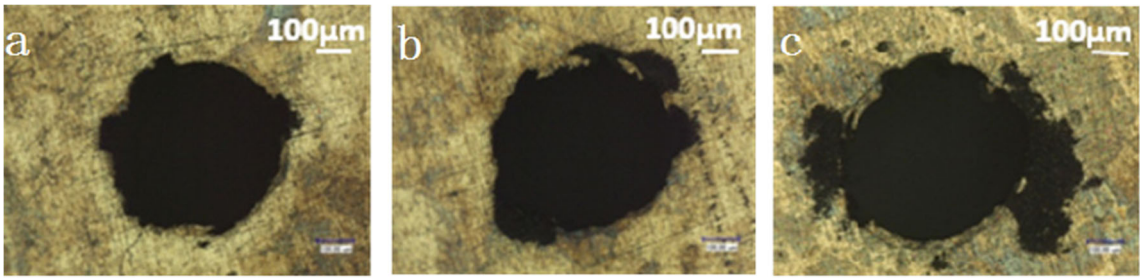

Fig. 15 The metallograph of some experimental holes

machining. Due to the smaller voltage, the stray corrosion of the orifice became weakened without an obvious over-cutting phenomenon. In addition, a lace phenomenon occurred in the orifice. The reaming hole edge was connected by several small circular arcs, and much of the orifice material was removed, while the recast layer of the hole wall remained. Thus, material removal during electrolysis was uneven, such that the recast layers could not be completely removed; they consistently left some dead angles. The electrolyte in the machining gap mixed continuously with hydrogen bubbles and electrolysis products, which led to greater change in composition and conductivity, and the chemical reaction was limited to a small area. The metallograph of some experimental holes obtained by continuous electrolysis is shown in Fig. 15, indicating that material removal at the outlet was more random and the surface was damaged to some degree.

In the above experiment, by adding a small amount of strong acid to the electrolyte, electrolytic products exist in the form of ions, avoiding a short circuit between the solid particles and the two poles and thus improving processing stability. However, the concentration polarization caused by the concentration of metal cations had a more obtrusive effect on the electrochemical reaction, which was not conducive to smooth electrolytic progress. Therefore, a periodic flushing method was adopted in hydrostatic electrolytic machining. The concentration of $NaNO_3$, electrolysis voltage, flushing numbers, and initial machining gap were maintained under technological parameters to conduct the orthogonal experiment. For each parameter, three levels were selected. Regardless of the interaction of each factor, $L_9(3^4)$ was used to designate the orthogonal experiment. Experimental factor levels are shown in Table 4.

Thirty prefabricated holes were drilled according to the optimized technological parameters. Three holes were processed in each group of parameters, and the average value was taken as the test result, after which the three reference holes were set. The rotary-cut diameter of the prefabricated holes was φ0.2, φ0.22, and φ0.25 mm, respectively. The tungsten electrode with an outer diameter of φ0.2 mm was used to form a different machining gap. According to preliminary experimental data, the electrolyte was added to 0.12 mol/L HCl (diluted 100 times) with a 30-s time interval for flushing to ensure the fluid flowed smoothly. After electrolysis, the reaming amount of the inlet was counted to investigate the degree of stray orifice corrosion; results are shown in Table 5.

Regarding orifice stray corrosion, the order of influence of each factor is as follows: electrolytic voltage > flushing numbers > electrolyte concentration > machining gap. Electrolysis voltage had an important impact on stray corrosion: the greater the voltage, the more serious the corrosion; thus, the optimal electrolytic voltage was 6 V. An increase in the flushing numbers indicates that the machining time was extended, resulting in easy renewal of the reaction environment and more serious stray corrosion. When the electrolyte concentration increased, the reaming amount of the inlet first increased

Table 4 Orthogonal experimental factors level

Level	Factor			
	A Concentration of $NaNO_3$ (g/L)	B Electrolytic voltage (V)	C Flushing numbers	D Machining gap (mm)
1	A1 = 12	B1 = 6	C1 = 6	D1 = 0.12
2	A2 = 15	B2 = 7	C2 = 8	D2 = 0.14
3	A3 = 18	B3 = 8	C3 = 10	D3 = 0.16

Table 5 The experimental results

Order number	A	B	C	D	The reaming amount of the inlet (μm)
1	1	1	1	1	66.21
2	1	2	2	2	126
3	1	3	3	3	148.04
4	2	1	3	2	22.04
5	2	2	1	3	209
6	2	3	2	1	126
7	3	1	2	3	35.1
8	3	2	3	1	150.04
9	3	3	1	2	28.1
Range (*R*)	47.93	120.56	72	11.01	–
Trend	↗↘	↗	↗	↘↗	–

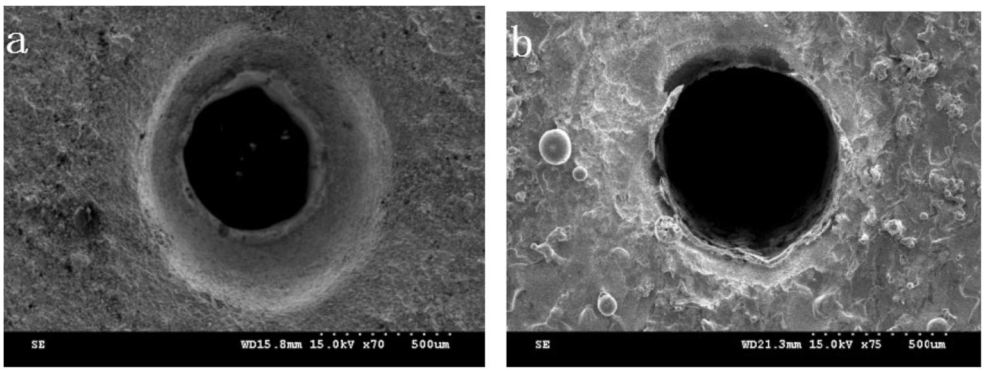

Fig. 16 The optimal experimental result. **a** Inlet. **b** Outlet

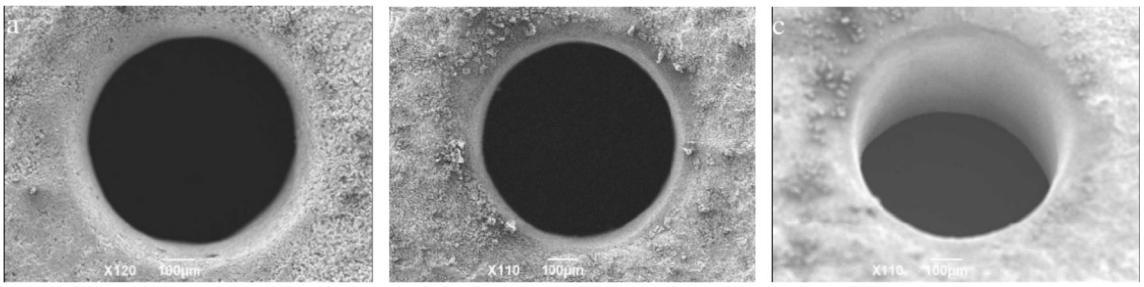

Fig. 17 Optimized hole morphology by forced flushing. **a** Inlet. **b** Outlet. **c** Side wall

and then decreased, attributable to the non-linearity of $NaNO_3$. An appropriately larger current density was beneficial to obtaining a better processing result. The machining gap had little effect on the reaming amount of the inlet.

Figure 16 shows the optimal experimental results. The parameters were an electrolyte concentration of 18 g/L, electrolytic voltage of 6 V, flushing numbers of 8, and machining gap of 0.16 mm. The hole circularity was good and the inner wall was smooth, leaving only a few recast layers near the exit, which attached to the hole wall and were not removed completely. When adopting the free flushing method, due to the large flow resistance around the hole outlet, the electrolyte renewed difficulty and could not effectively and promptly remove electrolytic products and depolarization. However, the recast layer was densely distributed, which made it difficult to remove completely. Considering that an increase in the flushing numbers would affect the hole taper, the entrance material would then be removed excessively, so forced flushing was adopted for optimization.

Table 6 Comparison of the aperture before and after forced flushing

	Inlet aperture (μm)	Outlet aperture (μm)	Taper
Reference hole	546.48	426.34	0.120
Experimental hole	765.54	618.41	0.147
Change quantity	+ 219.06	+ 192.07	+ 0.027

The morphology of a hole after electrolysis is shown in Fig. 17. This hole demonstrated excellent roundness, which improved the out-of-round phenomenon of the coarse hole shape caused by an interpolation track error when completing the rotary-cut small diameter. The inner wall was flat and smooth, the size of the outlet and inlet was similar, and the circular angle of each showed a gentle and natural transition with the matrix. The surrounding matrix surface exhibited almost no damage, and the processing mark of the linear cutting machining on the inlet surface was polished after electrolysis to reveal a bright and smooth surface. The burr at the outlet caused by laser drilling was also dissolved and removed.

The dimension comparison of the reference hole and experimental hole before and after forced flushing electrolysis is shown in Table 6. The hole taper was slightly higher than that before electrolysis, mainly because the liquid at the outlet was more difficult to renew than at the inlet, the liquid mass transfer step became the control step, and the electrolytic leveling effect could not be fully exerted. To uncover the principle of recast layer electrolytic removal and further optimize it using technological parameters, it was necessary to carry out a composite machining test under the machining conditions and technological process described above. The change rule of hole morphology under different machining times and conditions was researched; the flushing numbers were set to be 1–6. To increase experimental reliability, three holes with identical parameters were processed. The obtained experimental results

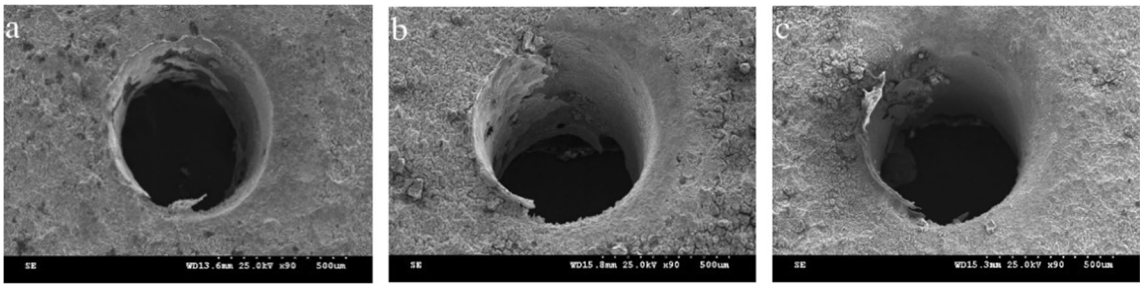

Fig. 18 Morphology of small hole at different flushing numbers. **a** 2. **b** 4. **c** 6

are shown in Fig. 18. The recast layers were removed along with the circumference via forced flushing. The material removal rate was more stable and easily controlled; it did not generate excessive reaming problems, unlike high-speed flushing outside the ring electrode. In hydrostatic machining, the dissolution of anode materials began from the minimum position of flushing resistance and then filled in the enlarged gap with the electrolyte. The recast layer adhered to the hole wall eroded slowly until the gap around the electrode was even. The surrounding dissolution rate gradually became balanced and could develop small holes with suitable roundness, which is an advantage of electrolytic machining. When the flushing number was 8, the recast layer around the hole was removed completely, the surrounding gap became balanced, and small holes with a round shape could be obtained with no recast layer and no surface damage.

6 Conclusion

In this study, laser-electrolytic composite machining technology was adopted to conduct a boring test on nickel-based superalloy In718 through flushing outside the ring electrode and hydrostatic machining. Based on experimental results, the following conclusions can be drawn:

1) To examine the laser rotary-cut boring method, this study carried out a boring test on In718 nickel-based superalloy using optimized laser pulse parameters and motion parameters. Results show that the recast layer exhibited a random distribution and gathered together at the exit.
2) For small holes with a diameter larger than 1 mm, electrolytic post-processing for the laser prefabricated small holes was conducted using high-speed flushing outside the ring electrode. The optimal technological parameters were as follows: electrolytic voltage of 20 V, $NaNO_3$ electrolyte of 7.5 g/L, electrolytic machining time of 20s, and a reaming amount between 70 and 100 μm. This method demonstrated a good machining effect and lent itself to steady recast layer removal.
3) For small holes with a diameter smaller than 1 mm, electrolytic post-processing for the small holes was conducted using hydrostatic machining. The continuous static electrolyte machining and free flushing could not achieve complete recast layer removal, whereas forced flushing could remove the recast layer. The optimal technological parameters were as follows: electrolytic voltage of 6 V, compound electrolyte of 18 g/L$NaNO_3$ + 2 g/LNaCl + 0.12 mol/LHCl, and flushing number of 8. This method obtained a small hole, which had a good hole shape and inner-wall quality, and the hole wall had no residual recast layer.

Funding information This research is supported by National 863 Program (2013AA040101).

Publisher's Note Springer Nature remains neutral with regard to jurisdictional claims in published maps and institutional affiliations.

References

1. Tagliaferri F, Genna S, Leone C, Palumbo B, De Chiara G (2017) Experimental study of fibre laser microdrilling of aerospace superalloy by trepanning technique. Int J Adv Manuf Technol 93:3203–3210. https://doi.org/10.1007/s00170-017-0773-4
2. Leone C, Genna S, Caggiano A, Tagliaferri V, Molitierno R (2016) Influence of process parameters on kerf geometry and surface roughness in Nd: YAG laser cutting of Al 6061T6 alloy sheet. Int J Adv Manuf Technol 87:2745–2762
3. Daxiang L, Jie J (2004) The development trends and prospect of world aero propulsion technology in the 21st century. Eng Sci 6(9):1–8
4. Guo W, Wang M, Xiaobing Z (2003) Recast layer formed by laser drilling of Ni-based superalloys and progress on its control. J Laser 24(4):1–3
5. Biffi CA, Previtali B (2013) Spatter reduction in nanosecond fibre laser drilling using an innovative nozze. Int J Adv Manuf Technol 66:1231–1245
6. Przestacki D, Kuklinski M, Bartkowska A (2017) Influence of laser heat treatment on microstructure and properties of surface layer of Waspaloy aimed for laser-assisted machining. Int J Adv Manuf Technol 93:3111–3123. https://doi.org/10.1007/s00170-017-0775-2
7. Changjun C, Wenyuan G, Maocai W, Xiaobing Z (2004) An experimental study on the chemical etching of the remelt layers formed on Ni-based superalloy. Gas Turbine Exp Res 17(3):44–50
8. Zhang Y, Xu Z, Di Zhu NQ (2016) Drilling of film cooling holes by a EDM/ECM in situ combined process using internal and side flushing of tubular electrode. Int J Adv Manuf Technol 83:505–517

9. Caiazzo F, Alfieri V, Corrado G, Argenio P (2017) Laser powder-bed fusion of Inconel 718 to manufacture turbine blades. Int J Adv Manuf Technol 93:4023–4031. https://doi.org/10.1007/s00170-017-0839-3
10. Jain VK, Lal GK, Kanetkar Y (2005) Stray current attack and stagnation zones in electrochemical drilling. Int J Adv Manuf Technol 26(5–6):527–536
11. Kurita T, Hattori M (2006) A study of EDM and ECM/ECM-lapping complex machining technology. Int J Mach Tools and Manuf 46(14):1804–1810
12. Low DKY, Li L, Byrd PJ (2003) Spatter prevention during the laser drilling of selected aerospace materials. J Mater Pro Technol 139(1–3):71–76
13. Xiao C, Rongqing X, Zhonghua S (2000) Influence of assisted gas on laser drilling. J Laser 21(6):44–46
14. Xiao C, Rongqing X, Zhonghua S (2004) Mechanisms of laser processing in water and air. J Nanjing Univ Sci Technol 28(3): 248–252
15. Zhu XS, Choi JW, Cole R, Ahn CH (2002) A new laser micromachining technique using a mixed-mode ablation approach. The Fifteenth IEEE International Conference on MICRO Electro Mechanical Systems. IEEE:152–155
16. Nguyen MD, Rahman M, Wong YS (2013) Modeling of radial gap formed by material dissolution in simultaneous micro-EDM and micro-ECM drilling using deionized water. Int J Mach Tools Manuf 66:95–101
17. Sibailly O, Manley J, Richerzhagen B (2003) Mixing laser and water-the use of new wavelengths in water jet-guided laser technology bodes well for applications for transparent material. Ind Laser Solut 18(12):18–19
18. LIUXIN (2014) Research on EDM-ECM combined machining process for small-hole without recast layer. Nanjing UNIVERSITY of Aeronautics and Astronautics, Nanjing
19. Datta M, Romankiw LT, Vigliotti DR, Gutfeld RJV (1989) Jet and laser-jet electrochemical micromachining of nickel and steel. J Electrochem Soc 136(8):2251–2256
20. Lescuras V, Andri JC, Lapicque F, Zouari I (1995) Jet electrochemical etching of nickel in a sodium chloride medium assisted by a pulsed laser beam. J App Electrochem 25(10):933–939
21. Lau WS, Yue TM, Wang M (1994) Ultrasonic-aided laser drilling of aluminum-based metal matrix composites. CIRP Annals-Manuf Technol 43(1):177–180
22. Lixin Y, Jiawen X, Jianshe Z (2013) Experimental study of machining characteristics in hybrid proceeding of JECM-LBM on nickel-based superalloy. China Mech Eng 24(3): 302–308
23. Zhang Y, Xu Z, Di Zhu JX (2015) Tube electrode high-speed electrochemical discharge drilling using low-conductivity salt solution. Int J Mach Tools Manuf 92:10–18
24. Huang SF, Zhu D, Zeng YB (2011) Micro-hole machined by electrochemical discharge machining (ECDM) with high speed rotating cathode. Manuf Sci Technol 295:1794–1799